VERSITA

OPTO-ELECTRONICS REVIEW **19**(4), 425–434

DOI: 10.2478/s11772-011-0041-3

Wavelet analysis of polarization maps of polycrystalline biological fluids networks

Y.A. USHENKO*

Correlation Optics Department, Chernivtsi National University, 2 Kotsyubinsky Str., 58012 Chernivtsi, Ukraine

The optical model of human joints synovial fluid is proposed. The statistic (statistic moments), correlation (autocorrelation function) and self-similar (Log-Log dependencies of power spectrum) structure of polarization two-dimensional distributions (polarization maps) of synovial fluid has been analyzed. It has been shown that differentiation of polarization maps of joint synovial fluid with different physiological state samples is expected of scale-discriminative analysis. To mark out of small-scale domain structure of synovial fluid polarization maps, the wavelet analysis has been used. The set of parameters, which characterize statistic, correlation and self-similar structure of wavelet coefficients' distributions of different scales of polarization domains for diagnostics and differentiation of polycrystalline network transformation connected with the pathological processes, has been determined.

Keywords: wavelet analysis, polarization, crystal, birefringence, statistic moments, correlation function.

1. Introduction

Among many directions of optical diagnostics of organic phase-inhomogeneous objects, a new technique – laser polarimetry has been formed within recent 10 years [1–13]. It enables to obtain information about optical anisotropy of phase-inhomogeneous objects in the form of coordinate distributions of the biological tissues (BT) azimuths and ellipticities of their object field polarization.

Specifically, the above mentioned model was used for finding and substantiating the interrelations between the ensemble of statistic moments of the 1st to 4th orders that characterize the orientation-phase structure (distribution of optical axes and phase shifts for directions of protein fibril networks) of birefringent BT architectonics and that of 2D distributions of azimuths and ellipticities of their laser images [1]. It was determined that the 3rd and the 4th statistic moments for coordinate distributions of ellipticities are the most sensitive to the change (caused by dystrophic and oncological processes) of optical anisotropy inherent to protein crystals [14,15]. On this basis, the criteria for early diagnostics of muscle dystrophy, pre-cancer states of connective tissue, collagenosis, etc. were determined [16,17].

However, application of statistical analysis to coordinate distributions for azimuths and ellipticities of polarization in BT laser images does not enable to estimate local changes in the structure of optically anisotropic networks formed from protein crystals. On the other hand, in many cases, the study of biological fluids (blood, urine, bile, synovial fluid, etc.) is more topical and accessible from the clinical viewpoint than the study of BT. Thereof, the task to develop new approaches to a local analysis of polarization-inhomogeneous images of biological fluids seems rather reasonable.

Our work is aimed at studying capabilities of the wavelet analysis in determination of statistical (statistical moments of the 1st to 4th orders) as well as fractal (fractal dimensionalities) parameters that characterize distributions of wavelet coefficients for images of synovial fluid taken from human joints with various pathologies by using the method [18,19].

2. Optical model of synovial fluid

As a base for modelling the optical properties of synovial fluid we use the conception of anisotropy observed in BT protein networks developed in Ref. 1:

- synovial fluid can be considered as a two-component amorphous-crystalline structure,
- optically isotropic is the homogeneous complex of hyaluronic acid with proteins, high amount of leukocytes, high content of whole protein and lactic acid on the background of a low glucose content,
- optically anisotropic – liquid-crystalline phase consisting of a set of optically uniaxial birefringent liquid crystals of various types, fibrin fibers, and collagen fibers.

Polarization properties of local optically coaxial biological crystal can be described with the following Mueller operator $\{z\}_u$ [14]

*e-mail: yuriyu@gmail.com

$$\{z\}_u = \begin{Vmatrix} 1 & 0 & 0 & 0 \\ 0 & z_{22} & z_{23} & z_{24} \\ 0 & z_{32} & z_{33} & z_{32} \\ 0 & z_{42} & z_{43} & z_{44} \end{Vmatrix}, \tag{1}$$

where

$$(z_{ik})_u = \begin{cases} z_{22} = \cos^2 2\rho + \sin^2 2\rho \cos\delta, \\ z_{23,32} = \cos 2\rho \sin 2\rho(1-\cos\delta), \\ z_{33} = \sin^2 2\rho + \cos^2 2\rho \cos\delta, \\ z_{34,43} = \pm \cos 2\rho \sin\delta, \\ z_{24,42} = \pm \sin 2\rho \sin\delta, \\ z_{44} = \cos\delta. \end{cases} . \tag{2}$$

Here, ρ is the direction of optical axis, $\delta = (2\pi/\lambda)\Delta nd$ is the phase shift introduced between the orthogonal components of the amplitude of laser wave with the length λ passing through the liquid crystal with the linear size of its geometrical section d and the birefringence index Δn.

The Mueller f_{ik} matrix elements of liquid-crystal network in the plane of synovial fluid layer are determined by the following algorithm

$$f_{ik} = \sum_{u=1}^{N} [z_{ik}(\rho,\delta)]_u , \tag{3}$$

where N is the finite number of liquid crystals.

The classical definition of the Mueller matrix $\{F\}$ for biological objects consists not only in the fact that it describes optical properties of their optically anisotropic component, but also in the fact that such mathematical operator completely characterizes the processes of transformation of the Stokes vector S by phase-inhomogeneous layers [2–6]

$$S^* = \{F\} S_0 . \tag{4}$$

Here, S_0, S^* are the Stokes vectors of illuminating and object beams.

For a more general state of elliptically polarized wave, the Stokes vector looks as follows [1]

$$S_0 = \begin{pmatrix} 1 \\ \cos 2\alpha_0 \cos 2\beta_0 \\ \sin 2\alpha_0 \cos 2\beta_0 \\ \sin 2\beta_0 \end{pmatrix}, \tag{5}$$

where α_0, β_0 are the azimuth and ellipticity of an electromagnetic wave.

Taking into account Eq. (2) to Eq. (5), the Stokes vector S^* can be written in a complete form as

$$S^* = \begin{pmatrix} 1 \\ S_2 \\ S_3 \\ S_4 \end{pmatrix} = \begin{pmatrix} 1 \\ f_{22}\cos 2\alpha_0 \cos 2\beta_0 + f_{23}\sin 2\alpha_0 \cos 2\beta_0 + f_{24}\sin 2\beta_0 \\ f_{32}\cos 2\alpha_0 \cos 2\beta_0 + f_{33}\sin 2\alpha_0 \cos 2\beta_0 + f_{34}\sin 2\beta_0 \\ f_{42}\cos 2\alpha_0 \cos 2\beta_0 + f_{43}\sin 2\alpha_0 \cos 2\beta_0 + f_{44}\sin 2\beta_0 \end{pmatrix} = \begin{pmatrix} 1 \\ \cos 2\alpha \cos 2\beta \\ \sin 2\alpha \cos 2\beta \\ \sin 2\beta \end{pmatrix}. \tag{6}$$

Being based on Eq. (6), we obtain expressions for determining the azimuth α and the ellipticity β of the object electromagnetic field polarization

$$\alpha = 0.5 arctg\left(\frac{S_3}{S_2}\right) \equiv G[f_{ik}(\rho,\delta), \alpha_0, \beta_0], \tag{7}$$

$$\beta = 0.5 \arcsin(S_4) \equiv Q[f_{ik}(\rho,\delta), \alpha_0, \beta_0]. \tag{8}$$

For the investigated samples, the following range of lateral dimensions (1–15 μm) in the plane of a sample is the most probable. Such geometry of the optical-anisotropic network forms the following probable range of the phase δ changes (0–90 deg).

It follows from the analysis of Eqs. (7) and (8) that the state of polarization (α, β) of each point $(r \equiv x, y)$ of the BT image is determined by corresponding the local orientation – phase (ρ, δ) parameters of crystalline network.

In other words, on the terms of coordinate heterogeneity of the distributions $\rho(r)$ and $\delta(r)$ in the plane of the BT layer, a certain polarizationally inhomogeneous image is formed with the distributions $\alpha(r)$ and $\beta(r)$ called as polarization maps (PM) [1].

Hereinafter (without less of analysis completeness), the polarization map of ellipticity, which is the most convenient for characterization of biological crystals birefringence, will be considered.

3. Wavelet approach to analysis of distributions for ellipticity of polarization of laser images inherent to synovial fluid

If a prototype function is taken as a specific wavelet function, possessing a finite base both in coordinate and frequency spaces, then one can expand into series the one-dimensional distribution of the ellipticity $\beta(x)$ for polarization [18,19]

$$\beta(x) = \sum_{a,b=-\infty}^{\infty} C_{ab} \Psi_{ab}(x) , \tag{9}$$

where $\Psi_{ab}(x) = \Psi(ax - b)$ is the base function formed from the function-prototype by the shifting b and the scaling a, while the coefficients of this expansion are determined as follows

$$C_{ab} = \int \beta(x) \Psi_{ab}(x) dx . \tag{10}$$

The result of this wavelet transformation for the one-dimensional distribution of polarization parameters is a two-dimensional array of the coefficients that are defined by the following relation

$$W(a,b)=\frac{1}{|a|^{1/2}}\int_{-\infty}^{+\infty} f(\beta)\Psi\left(\frac{x-b}{a}\right)dx. \qquad (11)$$

In our work, as a wavelet function we have used the so-called MHAT function, i.e., the second derivative of the Gaussian function. MHAT wavelet possesses a narrow energy spectrum and two moments (zero and first) that are equal to zero. It satisfies the analysis of complex signals rather well. The mathematical expression for the MHAT wavelet is of the following form

$$\Psi(x)=\frac{d^2}{dx^2}e^{-x^2/2}=(1-x^2)e^{-x^2/2}. \qquad (12)$$

The quantitative analysis of two-dimensional distributions of wavelet coefficients, Eq. (11), $W(a,b)$ was performed by means of estimation of the set of statistic, correlation, and self-similar analysis which characterizes the series of one-dimensional samplings $W(a=2,10,30;\ b=1,2,\ldots m)$.

To estimate $W(a=2,10,30;\ b=1,2,\ldots m)$ distributions for various scales a of the wavelet function ψ, we calculated the set of their statistical moments of the 1st to the 4th orders $M_{j=1;2;3;4}$ [1,14]

$$M_1=\frac{1}{m}\sum_{i=1}^{m}|W_i|,\quad M_2=\sqrt{\frac{1}{m}\sum_{i=1}^{m}W_i^2},$$
$$M_3=\frac{1}{M_2^3}\frac{1}{m}\sum_{i=1}^{m}W_i^3,\quad M_4=\frac{1}{M_2^4}\frac{1}{m}\sum_{i=1}^{m}W_i^4. \qquad (13)$$

To calculate autocorrelation functions of $W(a=2,10,30;\ b=1,2,\ldots m)$ related with wavelet coefficients for distributions of ellipticity of laser image polarization, we used the following expression [1,20]

$$R_{xx}(m)=\frac{1}{(n-m)\sigma^2}\sum_{t=1}^{n-m}[X_t-\mu][X_{t+m}-\mu]. \qquad (14)$$

Here, is the length of discrete sampling $W(a=2,10,30;\ b=1,2,\ldots m)=X_1, X_2,\ldots, X_n$; μ is the average value, σ^2 is the dispersion, and m,n are the positive integers.

The fractal (self-similar) analysis of $W(a=2,10,30;\ b=1,2,\ldots m)$ distributions was performed using calculation of the logarithmic dependences $\log S_{xx}(\omega)-\log d^{-1}$ for the power spectra $S_{xx}(\omega)$, which was calculated as a discrete Fourier transform of the corresponding autocorrelation function $R_{xx}(m)$ using the MatLab software [1,20,21]

$$S_{xx}(w)=\sum_{m=1}^{n}R_{xx}(m)e^{-j\omega m}, \qquad (15)$$

where ω are the normalized frequencies which correspond to the spatial frequencies ($\omega=d^{-1}$) determined by the geometrical sizes d of structural elements of polarization map (ellipticity distribution) for a biological layer.

The dependences $\log S_{xx}(\omega)-\log d^{-1}$ are approximated using the least-squares method by the curves $\Phi(\eta)$.

Classification of $W(a=2,10,30;\ b=1,2,\ldots m)$ distributions is performed using the following criteria offered in Refs. 22, 23, 24, and 25:

- these distributions are fractal (self-similar), on the condition that the slope angle has the constant value $\eta=const$ in the dependence $\Phi(\eta)$ within 2 or 3 decades in changing the sizes d,
- the distributions are multi-fractal, on the condition of availability of several constant values for slope angles in $\Phi(\eta)$,
- the distributions are random, if there is no stable slope angle in $\Phi(\eta)$ over the whole range of changing sizes d.

4. Optical scheme of polarimeter and technique of polarimetric investigations

Figure 1 shows the traditional optical scheme of a polarimeter for measuring the set of coordinate distributions for ellipticity of polarization of laser images inherent to human synovial fluid [26–29].

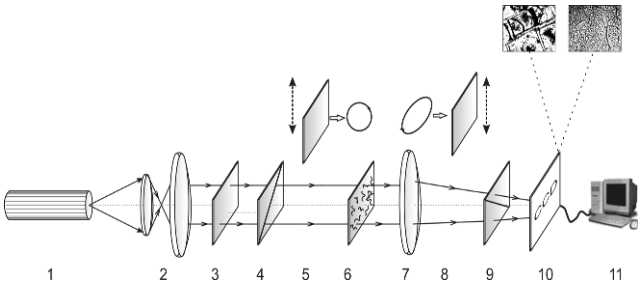

Fig. 1. Optical scheme of polarimeter: 1 – He-Ne laser, 2 – collimator, 3 – stationary quarter-wave plate, 5 and 8 – movable quarter-wave plates, 4 and 9 – polarizer and analyzer, respectively, 6 – object under investigation, 7 – micro-objective, 10 – CCD camera, and 11 – personal computer.

Illumination was made with a collimated beam (radius r = 10 mm) of He-Ne laser 1 (λ = 0.6328 μm). Using the polarization illuminator (quarter-wave plates 3, 5, and polarizer 4) we formed respective states for polarization of illuminating beam: 1 – 0°, 2 – 90°, 3 – 45°, 4 – ⊗ (right circulation).

The image of synovial fluid layer was formed within the light-sensitive area (800×600 pix) of CCD camera 10 by using the micro-objective 7.

For each separate pixel, we determined four parameters of the Stokes vector

$$S_1=I_0+I_{90},\quad S_2=I_0-I_{90},$$
$$S_3=I_{45}-I_{135},\quad S_4=I_{\otimes}-I_{\otimes}. \qquad (17)$$

Here, $I_0;I_{90};I_{45};I_{135}$ are the intensities of linearly (with the azimuths 0°, 90°, 45°, 135°) as well as the left- $I_{\otimes}$ and the right- $I_{\otimes}$ circularly polarized radiation transmitted by the system of the quarter-wave 8 – polarizer 9.

The values of ellipticity of polarization were calculated using the following algorithm

$$\beta(m \times n) = 0.5 \arcsin\left[\frac{S_4(m \times n)}{S_1(m \times n)}\right]. \qquad (18)$$

The coordinate sets of values $\beta(m \times n)$ we shall name as polarization maps.

5. Brief characteristic of objects under investigation

As objects for experimental studying, we chose optically--thin layers of synovial fluid taken from a joint of the healthy patient [Fig. 2(a)] and with atrophic arthritis [Fig. 2(b)].

The images of layers prepared from synovial fluid taken from human joints (Fig. 2) are indicative of availability of two fractions – optically isotropic and liquid-crystal network (anisotropic one). As it can be seen, geometric structure and sizes of separate elements in the polycrystalline network of the samples prepared from biological fluids are individual.

6. Polarization maps for laser images of human synovial fluid

Figure 3 illustrates the coordinate distributions of ellipticity $\beta(m \times n)$ [Figs. 3(a) and 3(e)] of polarization, histograms of distributions for their values $h(\beta)$ [Figs. 3(b) and 3(f)], the autocorrelation functions $K(\Delta x)$ for $\beta(m \times n)$ [Figs. 3(c) and 3(g)], as well as the logarithmic dependences $\log J(\beta) - \log d^{-1}$ [Figs. 3(d) and 3(h)] for polarization maps of synovial fluid taken from healthy [Figs. 3(a)–3(d)] and sick [Figs. 3(e)–3(h)] patients.

The analysis of the coordinate distributions for ellipticity $\beta(m \times n)$ [Figs. 3(a) and 3(e)] has shown that they contain two components:

- large-scale (100 to 300 μm) parts with homogeneous polarization (images of the optically isotropic component in human synovial fluid – homogeneous complex of hyaluronic acid with proteins, high amount of leukocytes, high content of whole protein and lactic acid on the background of a low glucose content) that coincides with that of laser beam $\beta^* = \beta_0 = 0^0$,
- polarization-inhomogeneous parts $\beta(\Delta x, \Delta y)$ = const – laser images of elements (2 to 50 μm) of optically

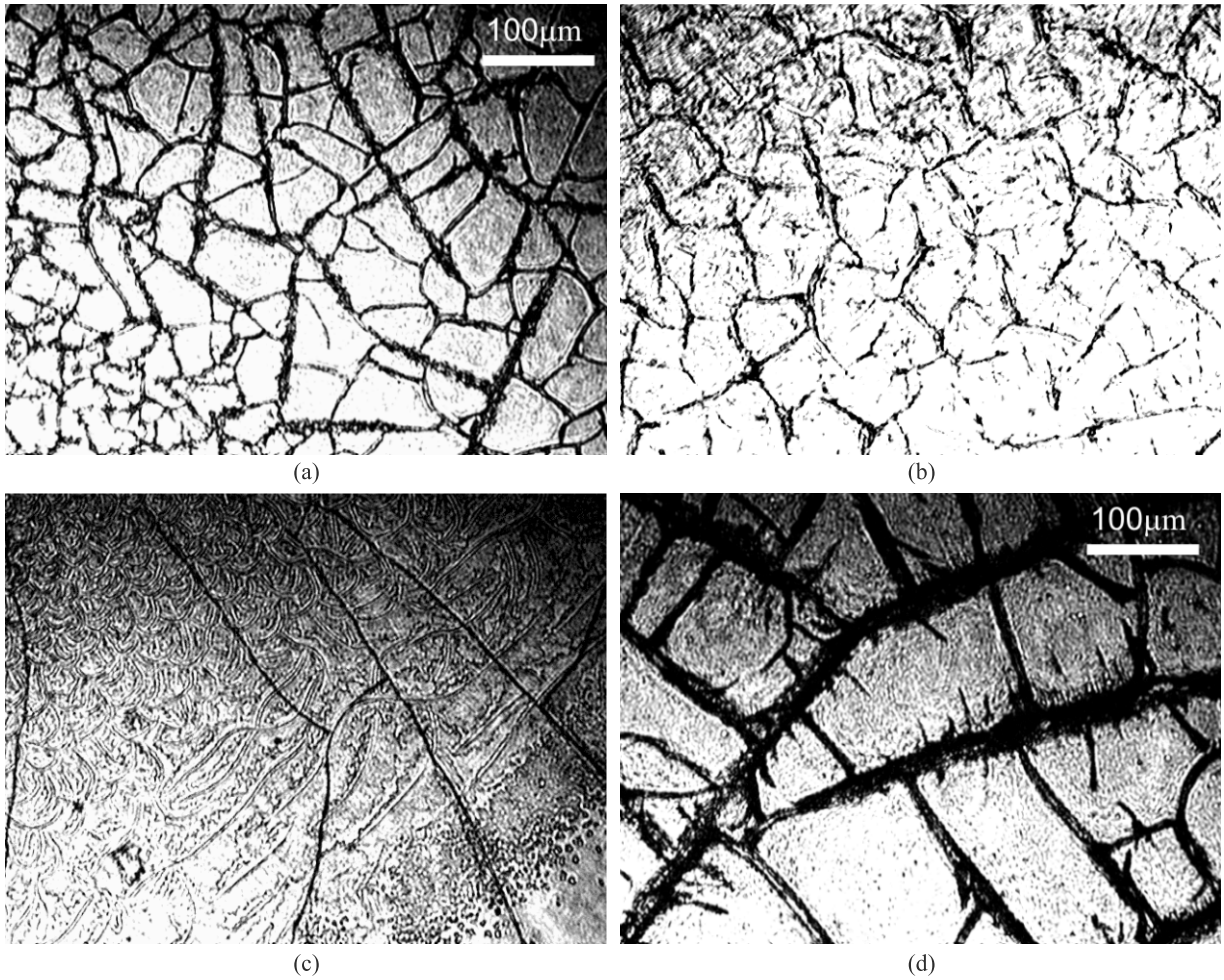

Fig. 2. Polycrystalline networks of synovial fluid taken from a joint of the healthy patient (a) and with atrophic arthritis of the final form (d). The intermediate stages of atrophic arthritis are shown in fragments (b, c).

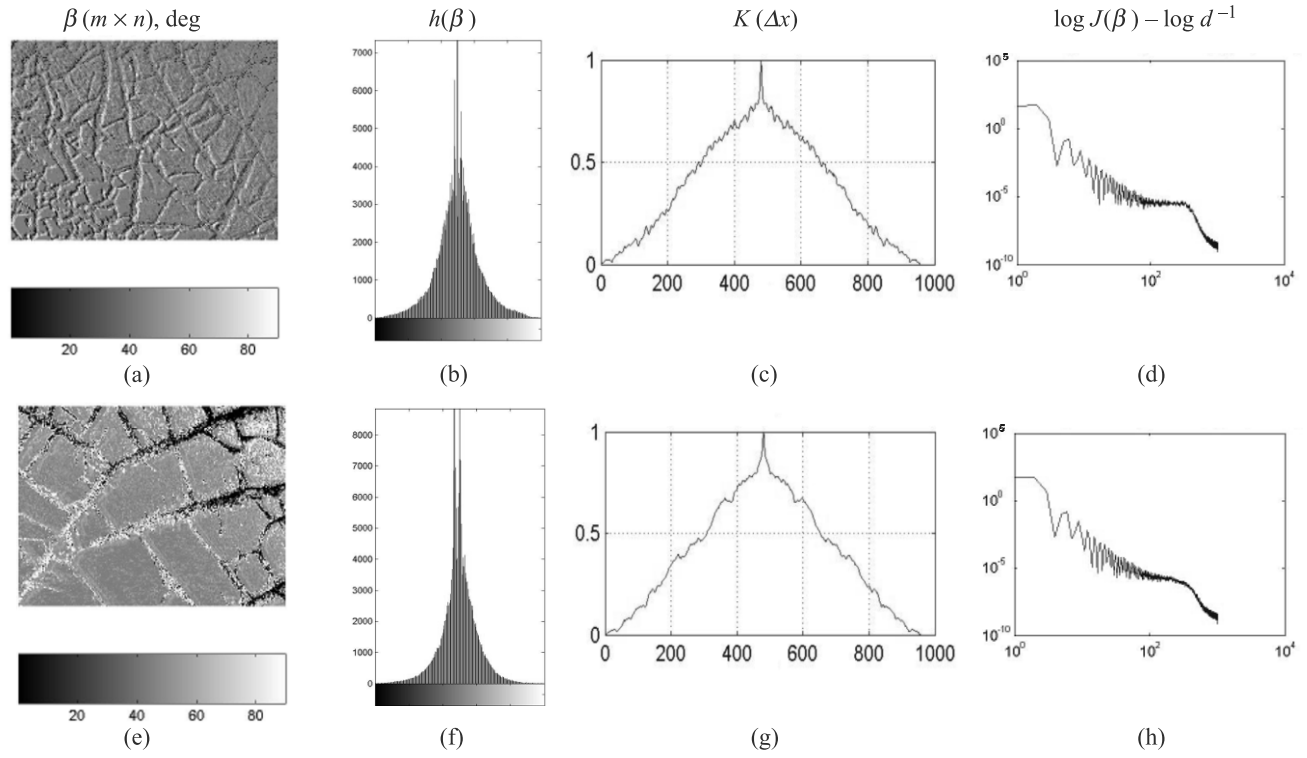

Fig. 3. Polarization maps for the ellipticity $\beta(m \times n)$ (a), (e), their statistical (b), (f), correlation (c), (g), and fractal (d), (h) parameters of synovial fluid taken from healthy [fragments (a) to (d)] and sick [fragments (e) to (h)] patients.

anisotropic – liquid-crystalline phase consisting of a set of optically uniaxial birefringent liquid crystals of various types, fibrin fibers and collagen fibers.

Quantitatively this structure of polarization maps for synovial fluid of both types can be illustrated with the histograms $h(\beta)$ that are dependences symmetrical relatively to the main extrema at $\beta = 0^{o}$.

Summarized in Table 1 are the values and ranges for statistical moments of the 1st to 4th orders that characterize the distributions $\beta(m \times n)$ within the limits of two groups of healthy ($q = 21$) and with atrophic arthritis ($q = 19$) patients.

Our comparative analysis of the data obtained did not reveal sufficiently reliable criteria (within the framework of statistical approach) for differentiation of coordinate structure in polarization maps for synovial fluid of both types. The values and ranges for changing the whole set of statistical moments $M_{j=1;2;3;4}$ related to distributions of the ellipticity β of polarization are superimposed.

Table 1. Statistical moments of the 1st to 4th orders for distributions of polarization parameters in laser images of human synovial fluid in different physiological states of patients.

$M_j(\beta)$	Norm ($q = 21$)	Atrophic arthritis ($q = 19$)
$M_1(\beta)$	0.05 ±0.006	0.06 ±0.008
$M_2(\beta)$	0.18 ±0.023	0.23 ±0.035
$M_3(\beta)$	0.78 ±0.081	0.64 ±0.069
$M_4(\beta)$	2.47 ±0.38	2.18 ±0.29

Correlation and self-similar analyses of polarization maps describing synovial fluid taken from healthy and sick patients revealed a fractal structure inherent to coordinate distributions of the ellipticity $\beta(m \times n)$ of polarization within the range of mean (50 to 200 μm) and large (200 to 2000 μm) geometrical sizes of biological crystals. The approximating curves $\Phi(\eta)$ for the dependences $\log J(\beta) - \log d^{-1}$ [Figs. 3(d) and 3(h)] are characterized with stable values of slope angles.

The main biochemical difference between such samples is the increase in globulin concentration, which forms small-scale optical-anisotropic network (≈2–50 μm). The estimation of such changes in polarization maps objectively is possible just only with the help of information selection by means of wavelet analysis.

In the field of small geometric sizes (2 to 50 μm) of the polycrystalline network in human synovial fluid, for all patients the values of fractal dimensionalities D_β for distributions of polarization parameters become indefinite. $\Phi_\beta(\eta)$ dependences within this range of sizes biological crystals are curve without any definite slope angle η(2….50 μm) ≠ const [Figs. 3(d) and 3(h)].

By other words, to determine a set of objective criteria for differentiation of polycrystalline networks of both types, one needs a more detailed analysis of polarization distributions just for these scales of geometrical sizes of biological crystals.

7. Wavelet analysis of polarization distributions of laser images for polycrystalline networks in synovial fluid

The locally scaled analysis of coordinate distributions $\beta(m \times n)$ for laser images of synovial fluid is provided using linear $k1,\ldots km$; $k = 1-n$ scanning by the MHAT wavelet with the step $b = 1$ pix and the window width 1 μm ≤ a_{min} ≤ 70 μm. The result of this scanning can be represented [see Eq. (11)] as a two-dimensional set of wavelet coefficients

$$W_{a,b} = \begin{pmatrix} W(a_{\min}, b_1) \cdot \cdot W(a_{\min}, b = m) \\ \cdot \quad \cdot \\ \cdot \quad \cdot \\ W(a_{\max}, b_1) \cdot \cdot W(a_{\max}, b = m) \end{pmatrix}$$

for each k^{th} line of pixels (Figs. 4 and 5) in the light-sensitive area of CCD 10 (Fig. 1).

Thus, the obtained set of wavelet coefficients $W(a_{\min}; b = k1–km)$ should be averaged using the following algorithm

$$\overline{W}_{a,b} = \begin{pmatrix} \overline{W}(a_{\min}, b_1) = \dfrac{\sum_{j=1}^{m} W_j(a_{\min}, b_1)}{m} \cdot \cdot \overline{W}(a_{\min}, b = m) = \dfrac{\sum_{j=1}^{m} W_j(a_{\min}, b_1 = m)}{m} \\ \cdot \quad \cdot \quad \cdot \\ \cdot \quad \cdot \quad \cdot \\ \overline{W}(a_{\max}, b_1) = \dfrac{\sum_{j=1}^{m} W_j(a_{\max}, b_1)}{m} \cdot \cdot \overline{W}(a_{\max}, b = m) = \dfrac{\sum_{j=1}^{m} W_j(a_{\max}, b_1 = m)}{m} \end{pmatrix} \tag{19}$$

The algorithm of Eq. (19) is an analogue of two-dimensional wavelet transformation that characterizes coordinate distributions for the ellipticity $\beta(m \times n)$ (Fig. 3) of polarization observed in laser images within the range of small scales 1 μm ≤ a_{min} ≤ 70 μm in polycrystalline structures of synovial fluid.

Figures 6 and 7 show the results of experimental investigations of correlation [autocorrelation functions $K(W_{a,b})$, – (b), (e), (h)] and fractal [logarithmic dependences of the power spectra $\log J(W_{a,b}) - \log d^{-1}$, – (c), (f), (m)] parameters that characterize the distributions $W(a_{\min}; b = k1 - km)$, – (a), (d), (g) for three scales $a_{\min}$ = 2 μm; 20 μm; 40 μm of the MHAT wavelet for polarization maps $\beta(m \times n)$ describing synovial fluids of a healthy (Fig. 6) and with atrophic arthritis (Fig. 7) patients.

As seen from the data obtained, the distributions for wavelet coefficients $\overline{W}[(a_{\min} = 2\mu m; 20\mu m; 40\mu m); (b = k1 \div km)]$ of polarization maps $\beta(m \times n)$ for the polycrystalline network of healthy patient's synovial fluid are individual for each scale $a_{\min}$ = 2 μm; 20 μm; 40 μm of the MHAT wavelet.

Our statistical analysis (Figs. 6 and 7, left columns) of the distributions $\overline{W}_{[(a_{\min} = 2\,\mu m;\ 20\mu m;\ 40\,\mu m);\ (b = k1 \div km)]}(\beta)$ revealed different dynamics for changing the values $M_{j=1;2;3;4}$ with increasing the scale $a_{\min}$ of the MHAT wavelet. The ranges of changes in statistical moments of the 1st to the 4th orders lie within the limits of M_3 = 1.7–3.6 and M_4 = 2.3–7.2 times, respectively. The found tendency is indicative of transformation observed for distributions of wavelet coefficients from practically random ($M_{1;2} >> M_{3;4} \to 0$) up to the stochastic ones ($M_{3;4} >> M_{1;2}$) [14].

This fact is also confirmed by the dependences (Figs. 6 and 7, central columns) of the autocorrelation functions $K\{W_{[(a_{\min} = 2\,\mu m; 20\mu m; 40\mu m); (b = k1 \div km)]}(\beta)\}$ for the distributions of wavelet coefficients, as they are superposition of two components, namely statistical that drops monotonically, and the oscillating one that is caused by periodical coordinate changes in these distributions.

The revealed features of statistical and coordinate structures in distributions of wavelet coefficients for polarization maps describing healthy patient's synovial fluids are related, in our opinion, with a different degree of self-similarity in distributions of the optical axis directions ρ and the phase shifts δ in polycrystalline structures at different scales of analysis $a_{\min}$ = 2 μm; 20 μm; 40 μm of the MHAT wavelet.

So, for small scales ($a_{\min}$ = 2 μm), a dominant contribution to formation of the coordinate distributions $\beta(m \times n)$ is caused by chaotically oriented crystals [Figs. 2(a) and 2(b)]. Therefore, just the random component dominates in the respective distributions for the wavelet coefficients $\overline{W}_{[(a_{\min} = 2\,\mu m;\ (b = k1 \div km)]}(\beta)$.

When the scale grows $a_{\min}$ = 20 μm; 40 μm, also growing is the contribution to formation of distributions for polarization parameters of the set oriented along directions of optical axes of albumin crystals [Figs. 2(a) and 2(b)]. From the statistical viewpoint, this process should be observed in the growth of statistical moments of the 3rd and 4th orders that characterize the distributions $\overline{W}_{[(a_{\min} = 20\mu m;\ 40\mu m);\ (b = k1 \div km)]}(\beta)$, as well as in formation of oscillations of autocorrelation dependences $K\{\overline{W}(\beta)\}$.

Besides, some stable slope η of approximating curves $\Phi(\eta)$ for $a_{\min}$ = 2 μm in the logarithmic dependences $\log J[W_{a,b}(\beta)] - \log d^{-1}$ is absent. The growth in the scale $a_{\min}$ = 20 μm; 40 μm of the MHAT wavelet can be observed in transformation of the random curves $\Phi(\eta)$ into polygonal lines [Figs. 6 and 7, right columns)] In other words, the random distributions $\overline{W}_{[(a_{\min} = 2\,\mu m;\ (b = k1 \div km)]}(\beta)$ are transformed into the multi-fractal ones.

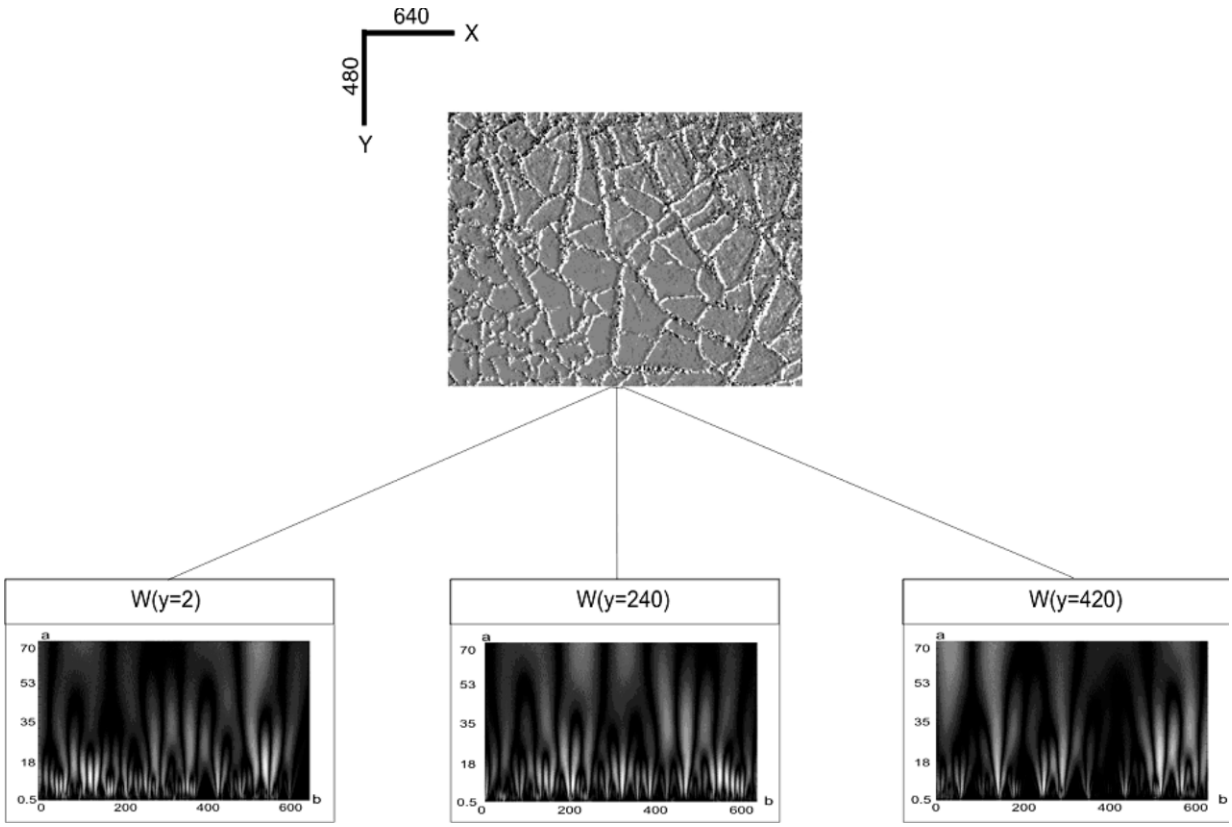

Fig. 4. Distributions of wavelet coefficients $W(a_{\min}; b = k1–km)$ of the polarization map for ellipticity of polarization inherent to synovial liquid of a healthy patient for various lines k = 2;240;420 of CCD camera.

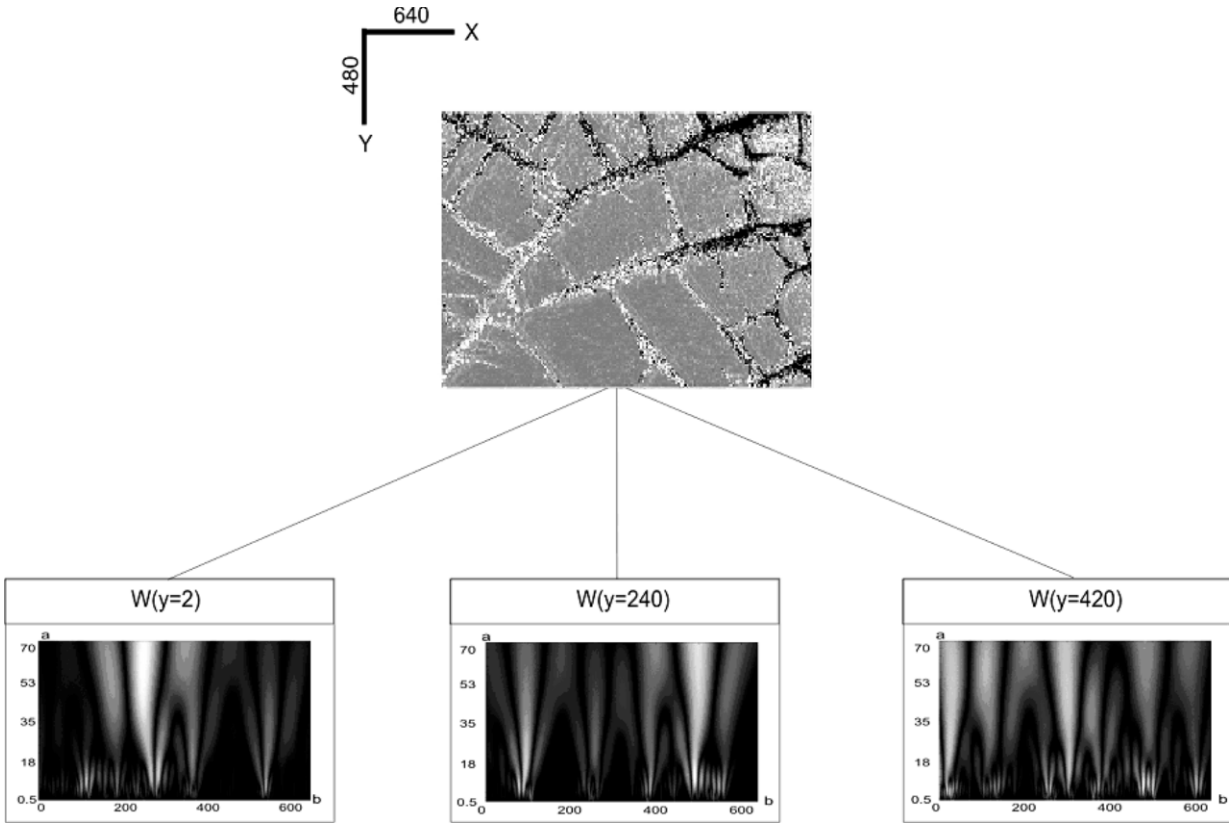

Fig. 5.Distributions of the wavelet coefficients $W(a_{\min}; b = k1 - km)$ of the polarization map for the ellipticity $\beta(m \times n)$ of polarization observed in synovial fluid of a patient with atrophic arthritis for various lines k = 2;240;420 of CCD camera.

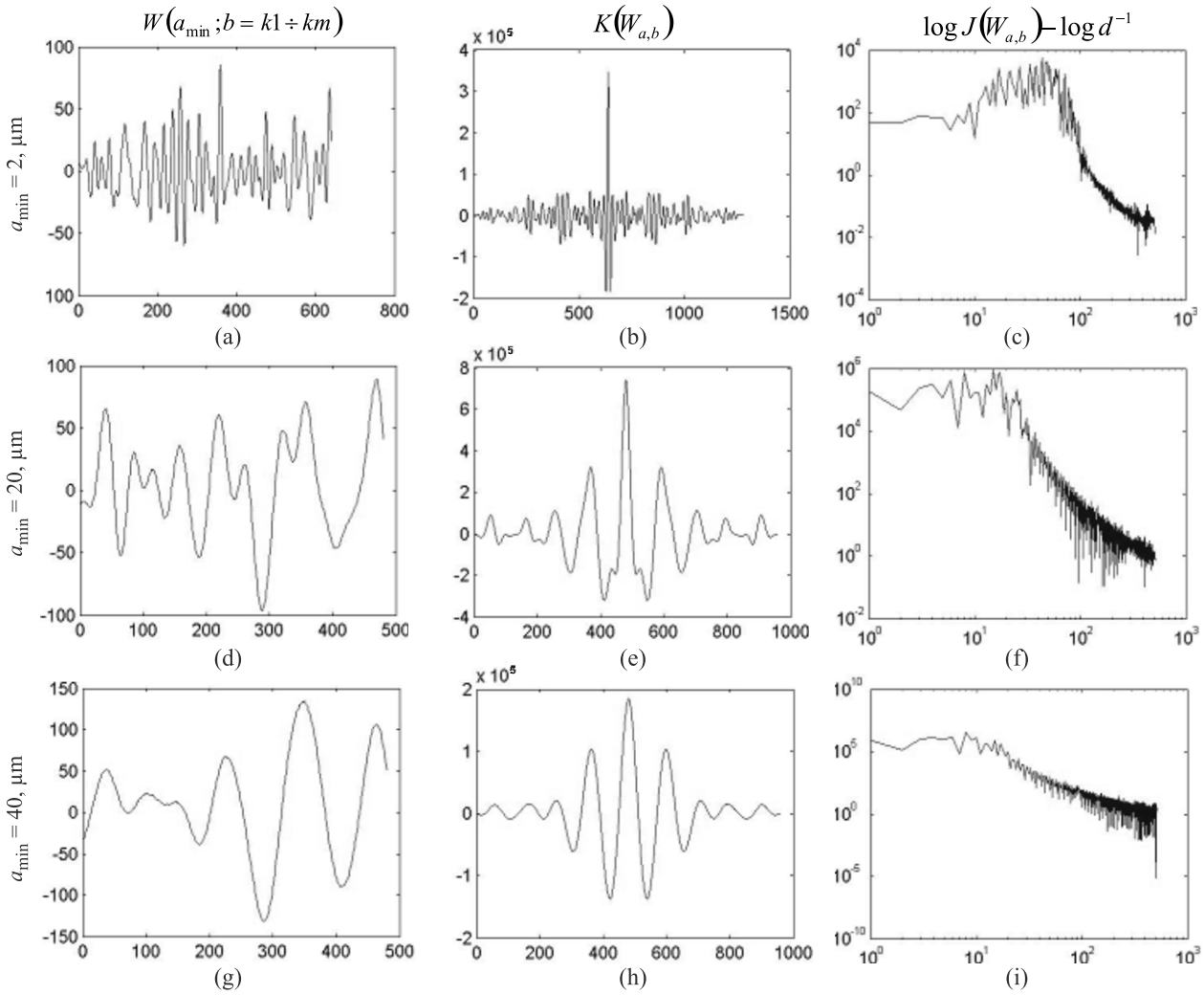

Fig. 6. Statistical (left column), correlation (central column) and fractal (right column) parameters of distributions inherent to the wavelet coefficients the polarization map for the ellipticity of a healthy patient's synovial fluids.

Our analysis of the data obtained for statistical, correlation and fractal parameters that characterize the sets of wavelet coefficients for various scales of MHAT functions for distributions of the ellipticity $\beta(m \times n)$ of laser images of the synovial fluid of a patient with atrophic arthritis enabled us to find:

- weak changes (within 15 to 25%) of the values of statistical moments $M_{j=1;2;3;4}$ that characterize the distributions $\overline{W}_{[(a_{\min}=2\,\mu m;\ (b=k1\div km)]}(\beta)$ on the scales $a_{\min}$ = 2 μm of the MHAT wavelet as compared with analogous statistical parameters determined for polarization maps of healthy patient's synovial fluid,
- an essential decrease in statistical moments of the 3rd (2.1 to 3.2 times) and 4th (2.4 to 3.7 times) orders for the distributions $\overline{W}_{[(a_{\min}=20\mu m;\ 40\mu m);\ (b=k1\div km)]}(\beta)$ determined on larger scales $a_{\min}$ = 20 μm; 40 μm of the MHAT wavelet,
- the absence of any stable slope of the approximating curves $\Phi(\eta)$ for the logarithmic dependences $\log J[W_{a,b}(\beta)] - \log d^{-1}$ determined on all the scales of the MHAT wavelet.

The above-mentioned differences between statistical moments and logarithmic dependences that characterize the distributions $\overline{W}_{[(a_{\min}=20\mu m;\ 40\mu m);\ (b=k1\div km)]}(\beta)$ can be related with growth of the optically anisotropic components in synovial fluid of a patient with atrophic arthritis. This biochemical process results in growth of the birefringence coefficient for partial biological crystals disordered as to directions of their optical axes. Moreover, this transformation of the polycrystalline structure begins from small sizes (d = 1–50 μm) of structural elements in the polycrystalline network. From the viewpoint of polarization, these processes become apparent via formation of random distributions for the ellipticity $\beta(m \times n)$ in respective synovial fluid laser images. It results in decrease in the values inherent to statistical moments of the 3rd and 4th orders that characterize the distributions $\overline{W}_{[(a_{\min}=2\,\mu m;\ 20\mu m;\ 40\mu m);\ (b=k1\div km)]}(\beta)$ on all the scales $a_{\min}$ of the MHAT wavelet [Figs. 6 to 7, left columns). Due to the same reason, the approximating curves $\Phi(\eta)$ for the logarithmic dependences $\log J[W(\beta)] - \log d^{-1}$ are characterized with the absence of a stable slope angle (Figs. 6 to 7, right columns).

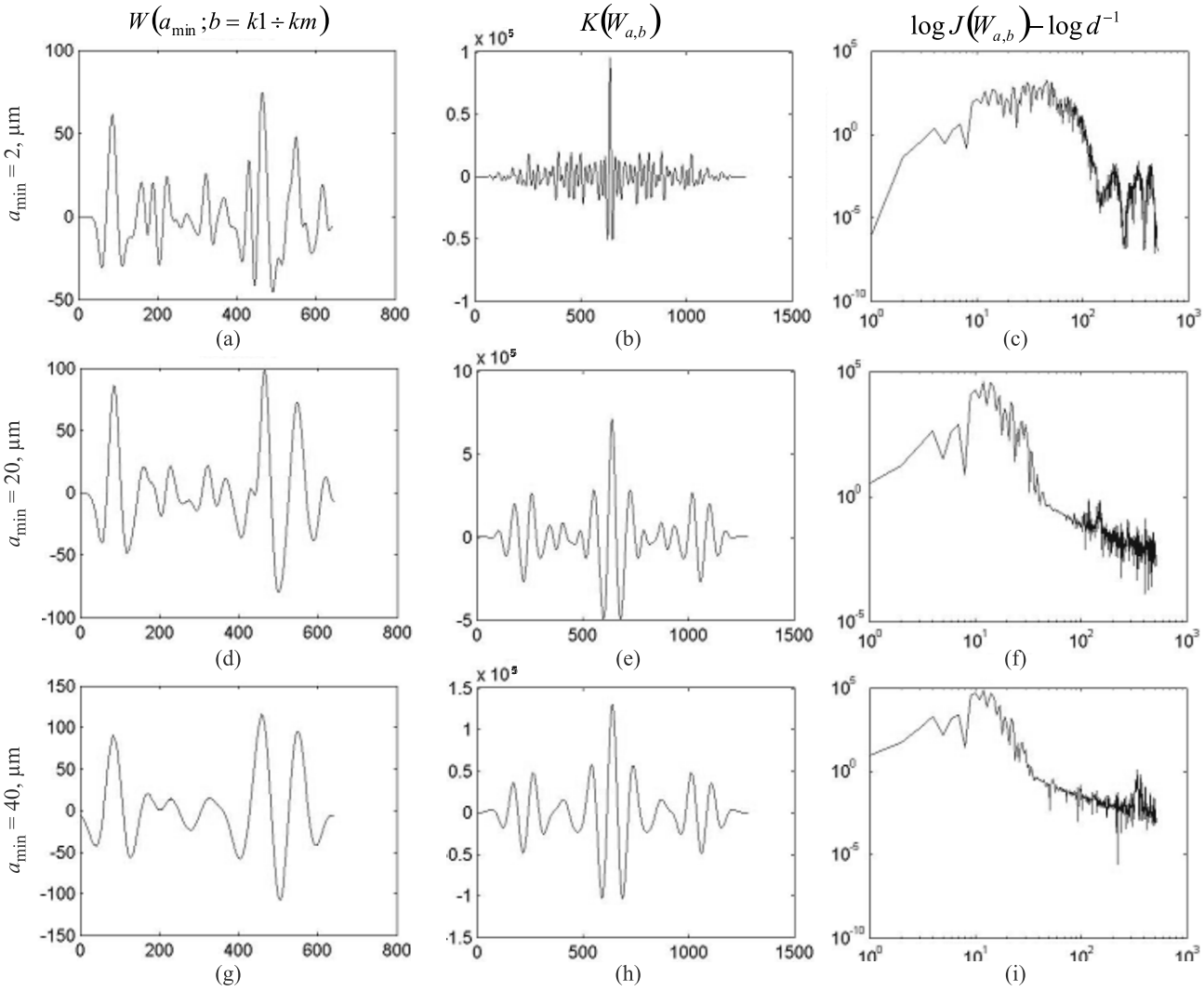

Fig. 7. Statistical (left column), correlation (central column) and fractal (right column) parameters of distributions inherent to the wavelet coefficients describing the polarization map for the ellipticity of atrophic arthritis patient's synovial fluids.

The possibilities of diagnosing pathological processes in a human organism by using the wavelet analysis of polarization maps for ellipticity of laser images describing synovial fluid have been illustrated in Table 2, where the values of statistical moments that characterize distributions on three scales $a_{\min}$ of the MHAT wavelet for two groups of healthy (21 samples) and sick (19 samples) patients are summarized.

8. Conclusions

- two-component optical model of synovial fluid is analytically proposed and experimentally substantiated,
- main transformation mechanisms of laser radiation polarization structure of polycrystalline networks of synovial fluid planar layers are defined,
- it has been shown that polarimetric diagnostics of synovial fluid biological crystal networks of different physiological states is ambiguous and demands of scale-discriminative wavelet analysis,

Table 2. Statistical moments of the 1st to the 4th orders for distributions of wavelet coefficients related to polarization maps for the ellipticity of laser images describing synovial fluid of healthy and with atrophic arthritis patients.

a_{min} (μm)	M_j	$\beta(m \times n)$	
		Norm	Atrophic arthritis
2	M_1	0.18 ±0.021	0.21 ±0.031
	M_2	0.27 ±0.038	0.24 ±0.035
	M_3	0.11 ±0.015	0.1 ±0.014
	M_4	0.07 ±0.008	0.05 ±0.0056
20	M_1	0.31 ±0.037	0.32 ±0.036
	M_2	0.18 ±0.025	0.16 ±0.0019
	M_3	0.33 ±0.041	0.14 ±0.018
	M_4	0.41 ±0.045	0.19 ±0.027
40	M_1	0.44 ±0.051	0.46 ±0.055
	M_2	0.12 ±0.14	0.1 ±0.012
	M_3	0.49 ±0.056	0.19 ±0.021
	M_4	0.81 ±0.093	0.22 ±0.047

- a set of objective criteria (statistic moments of the 3rd and the 4th orders, the degree of self-similarity of wavelet coefficients on different scales of polarization domains) for early diagnostics and differentiations of synovial fluid pathological transformations is determined.

References

1. A.G. Ushenko and V.P. Pishak, "Laser polarimetry of biological tissue: Principles and applications", in *Handbook of Coherent-Domain Optical Methods: Biomedical Diagnostics, Environmental and Material Science*, Vol. 1, pp. 93–138, edited by V.V. Tuchin, Kluwer Academic Publishers, 2004.
2. A.G. Ushenko, "Polarization structure of laser scattering fields", *Opt. Eng.* **34**, 1088–1093 (1995).
3. X. Wang, G. Yao, and L.V. Wang, "Monte Carlo model and single-scattering approximation of polarized light propagation in turbid media containing glucose", *Appl. Opt.* **41**, 792–801 (2002).
4. A.G. Ushenko, "Laser diagnostics of biofractals", *Quantum Electron.* **29**, 1078–1084 (1999).
5. S. Jiao, G. Yao, and L.V. Wang, "Depth-resolved two-dimensional Stokes vectors of backscattered light and Mueller matrices of biological tissue measured with optical coherence tomography", *Appl. Opt.* **39**, 6318–6324 (2000).
6. S. Jiao and L.V. Wang, "Two-dimensional depth-resolved Mueller matrix of biological tissue measured with double--beam polarization-sensitive optical coherence tomography", *Opt. Lett.* **27**, 101–103 (2002).
7. A.G. Ushenko, "The vector structure of laser biospeckle fields and polarization diagnostics of collagen skin structures", *Laser Phys.* **10**, 1143–1149 (2000).
8. S.G. Demos and R.R. Alfano, "Optical polarization imaging", *Appl. Opt.* **36**, 150–155 (1997).
9. A.G. Ushenko, "The vector structure of laser biospeckle fields and polarization diagnostics of collagen skin structures", *Laser Phys.* **10**, 1143–1149 (2000).
10. A.G. Ushenko, "Polarization correlometry of angular structure in the microrelief pattern of rough surfaces", *Opt. Spectrosc.* **92**, 227–229 (2002).
11. J.F. de Boer, T.E. Milner, M.J.C. van Gemert, and J.S. Nelson, "Two-dimensional birefringence imaging in biological tissue by polarization-sensitive optical coherence tomography", *Opt. Lett.* **22**, 934–936 (1997).
12. O.V. Angel'skii, A.G. Ushenko, A.D. Arkhelyuk, S.B. Ermolenko, and D.N. Burkovets, "Structure of matrices for the transformation of laser radiation by biofractals", *Quantum Electron.* **29**, 1074–1077 (1999).
13. A.G. Ushenko, "Polarization structure of biospeckles and the depolarization of laser radiation", *Opt. Spectrosc.* **89**, 597–601 (2000).
14. A.G. Ushenko, I.Z. Misevich, V. Istratiy, I. Bachyns'ka, A.P. Peresunko, O.K. Numan, and T.G. Moiysuk, "Evolution of statistic moments of 2D-distributions of biological liquid crystal net Mueller matrix elements in the process of their birefringent structure changes", *Advances in Optical Technologies*, doi: 10.1155/2010/423145.
15. O.V. Angelsky, A.P. Maksimyak, P.P. Maksimyak, and S.G. Hanson, "Optical correlation diagnostics of rough surfaces with large surface inhomogeneities", *Opt. Express* **14**, 7299–7311 (2006).
16. O.V. Angelsky, A.G. Ushenko, and Ye.G. Ushenko, "Investigation of the correlation structure of biological tissue polarization images during the diagnostics of their oncological changes", *Phys. Med. Biol.* **50**, 4811–4822 (2005).
17. O.V. Angelsky, A.G. Ushenko, and Ye.G. Ushenko, "2-D stokes polarimetry of biospeckle tissues images in pre-clinic diagnostics of their pre-cancer states", *J. Holography Speckle* **2**, 26–33 (2005).
18. O.V. Angelsky, G.V. Demianovsky, A.G. Ushenko, D.N. Burkovets, and Yu.A. Ushenko, "Wavelet analysis of two--dimensional birefringence images of architectonics in biotissues for diagnosing pathological changes", *J. Biomed. Opt.* **9**, 679–690 (2004).
19. O.V. Dubolazov, A.G. Ushenko, V.T. Bachynsky, A.P. Peresunko, and O.Ya. Vanchulyak, "On the feasibilities of using the wavelet analysis of Mueller matrix images of biological crystals", *Advances in Optical Technologies*, doi: 10.1155/2010/162832.
20. O.V. Angelsky, A.G. Ushenko, Yu.A. Ushenko, Ye.G. Ushenko, Yu.Ya. Tomka, and V.P. Pishak, "Polarization--correlation mapping of biological tissue coherent images", *J. Biomed. Opt.* **10**, article ID 064025 (2005).
21. B.B. Mandelbrot, *The Fractal Geometry of Nature*, San Francisco, W.H. Freeman, 1982.
22. O.V. Angelsky, Yu.Ya. Tomka, A.G. Ushenko, Ye.G. Ushenko, and Yu.A. Ushenko, "Investigation of 2D Mueller matrix structure of biological tissues for pre-clinical diagnostics of their pathological states", *J. Phys. D: Appl. Phys.* **38**, 4227–4235 (2005).
23. O.V. Angelsky, D.N. Burkovets, A.V. Kovalchuk, and S.G. Hanson, "Fractal description of rough surfaces", *Appl. Opt.* **41**, 4620–4629 (2002).
24. O.V. Angelsky, P.P. Maksimyak, and T.O. Perun, "Optical correlation method for measuring spatial complexity in optical fields", *Opt. Lett.* **18**, 90–92 (1993).
25. O.V. Angelsky, P.P. Maksimyak, and T.O. Perun, "Dimensionality in optical fields and signals", *Appl. Opt.* **32**, 6066–6071 (1993).
26. O.V. Angelsky, A.G. Ushenko, Y.G. Ushenko, and Y.Y. Tomka, "Polarization singularities of biological tissues images", *J. Biomed. Opt.* doi: 10.1117/1.2360527.
27. A.G. Ushenko, "Laser probing of biological tissues and the polarization selection of their images", *Opt. Spectrosc.* **91**, 932–936 (2001).
28. A.G. Ushenko, "Correlation processing and wavelet analysis of polarization images of biological tissues", *Opt. Spectrosc.* **91**, 773–778 (2002).
29. A.G. Ushenko, "Laser polarimetry of polarization-phase statistical moments of the object field of optically anisotropic scattering layers", *Opt. Spectrosc.* **91**, 313–316 (2001).

